Design and Modeling of a Hydraulically Amplified Magnetostrictive Actuator for Automotive Engine Mounts

Suryarghya Chakrabarti, Marcelo J. Dapino

Smart Vehicle Concepts Center, The Ohio State University, Columbus, OH, USA, 43210

ABSTRACT

A bidirectional magnetostrictive actuator with millimeter stroke and a blocked force of few tens of Newtons has been developed based on a Terfenol-D driver and a simple hydraulic magnification stage. The actuator is compared with an electrodynamic actuator used in active powertrain mounts in terms of electrical power consumption, frequency bandwidth, and spectral content of the response. The measurements show that the actuator has a flat free-displacement and blocked-force response up to 200 Hz, suggesting a significantly broader frequency bandwidth than commercial electromagnetic actuators while drawing comparable amounts of power.

Keywords: Terfenol-D, active mount, magnetostrictive, active vibration isolation

1. INTRODUCTION

A typical automotive engine mount has two main purposes. The first is to isolate the engine vibrations from the chassis; the second purpose is to prevent engine bounce from shock excitations primarily arising from the road. The frequency range of engine vibrations depends on the number of cylinders in the engine, the stroke number and the engine speed. It has been established that for a four-cylinder, four-stroke engine the frequency of engine vibrations ranges from 20-200 Hz for engine speeds of 600-6000 rpm.[1] For an eight-cylinder engine the frequency of vibrations would be 40-400 Hz for the same range of engine speeds. In order for the mount to be effective in isolating engine vibrations from the chassis, it should be compliant and lightly damped to reduce force transmissibility. The road excitations and other forms of shock excitations like sudden acceleration and braking typically occur below 5 Hz. To prevent engine bounce due to such excitations, the mount should be stiff and heavily damped.

To be able to address these contradicting requirements, an effective mount must have frequency and amplitude dependent characteristics. Various passive and semi-active mounts have been developed which are capable of significant vibration reduction (see, e.g., Yu et al.[1] and Jazar et al.[2]). Despite these advances, the trend of increased engine power combined with lighter vehicle frames poses vibration isolation problems which passive mounts cannot adequately address. Hence, significant emphasis is now placed on investigating designs and methods to develop effective active mounts. Lee et al.[3] developed an electromagnetic actuator with a bandwidth of 75 Hz. Gennesseaux[4] discusses a variable reluctance linear electric motor with in-built close loop control to address actuator nonlinearities. Although active mounts with electromagnetic actuators can achieve significant vibration reduction , their performance is restricted to low frequencies, typically below 80 Hz. Actuators capable of broader frequency bandwidth are thus necessary.

Most of the smart material induced-strain actuators capable of broadband response have a very limited stroke with peak strains on the order of 1200 ppm. Given the size restrictions of the automotive mount, a displacement amplification mechanism is necessary when employing smart materials. Niezrecki et. al.[5] have summarized some of the displacement amplification techniques found in the literature. Mechanisms such as stacking and mechanical levers are too bulky to be used in an active mount. Another way to amplify the motion of smart material actuators is by using a hydraulic fluid. A common way of hydraulic amplification is to use pistons of different areas with the smart material driving the large piston and the power output delivered by the smaller driven piston. Yoon et al.[6] developed one such actuator driven by a piezoelectric stack. Their device achieved

Further author information: (Send correspondence to M.J.D)
S.C.: E-mail: chakrabarti.3@osu.edu, Telephone: 1-614-247-7480
M.J.D.: E-mail: dapino.1@osu.edu, Telephone: 1-614-688-3689

Industrial and Commercial Applications of Smart Structures Technologies 2009,
edited by Benjamin K. Henderson, M. Brett McMickell, Proc. of SPIE Vol. 7290, 72900D
 · doi: 10.1117/12.817019

a unidirectional stroke of around 1.3 mm with a blocked force of ≈ 6.5 N. Hydraulic amplification can also be achieved by using smart material pumps driven at high frequency along with fluid rectification valves. Various pumps have been developed using both magnetostrictive[7,8] and piezoelectric materials.[9–11] The current designs are too bulky and complex for use in engine mounts due to the presence of various pumping components, an accumulator, check valves, direction control valve and a piston type hydraulic actuator. Hence, direct hydraulic amplification mechanisms are more attractive for designing smart material actuators for automotive engine mounts. Ushijima and Kumakawa[12] developed a piezohydraulic actuator with a stroke of 70 μm which takes advantage of the hydraulic fluid in the mount for amplification. Shibayama et al.[13] developed a hydraulically amplified piezo actuator having a stroke of 0.3 mm with considerable reduction in vibration transmission. The hydraulic fluid used for amplification was separately sealed from the fluid in the mount. However, the required voltages are very large.

The objectives of this study are to design, test, and model a compact bidirectional magnetostrictive actuator coupled with a hydraulic gain to be used as an actuator in active engine mounts. Section 2 describes the design aspects of the actuator. In section 3, the actuator is tested in mechanically-free and blocked conditions and its response is compared to that of a commercial electrodynamic actuator currently used in active mounts. The performances are compared in terms of electrical power consumption, frequency bandwidth and spectral content. Section 4 presents the nonlinear modeling of the actuator's dynamic response.

2. ACTUATOR DESIGN

2.1 Estimation of actuator requirements

The first step is to quantify the actuator requirements of a generic active mount. This is done by using a model similar to that developed by Lee et al.[3] (Figure 1). In this model, the transfer function of the actuator displacement to the engine displacement is given by

$$\frac{X_d}{X}(s) = \left[\left(1 + \frac{K_r}{K_b}\right)\frac{A_e}{A_d} + \frac{K_r A_t^2}{A_e A_d\left(ms^2 + cs + K_\epsilon\right)}\right]. \tag{1}$$

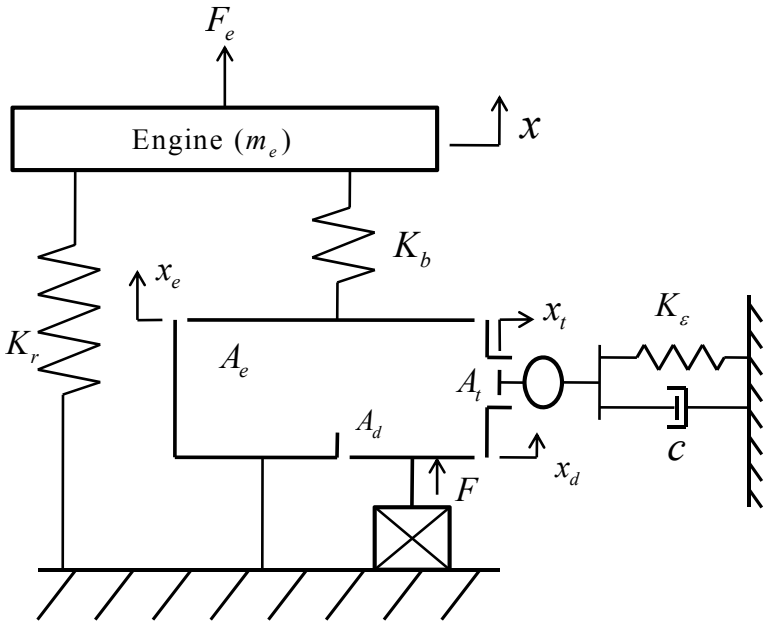

Figure 1. Schematic of the active mount model (Lee et. al.[3]).

Table 1 summarizes the values of the parameters used in our simulations, which coincide with the parameters used by Lee et al.[3] Figure 2 shows the magnitude of the frequency response. The response remains almost constant in the frequency range from 100 to 1000 Hz. To estimate the actuator displacement requirement from this plot, it is first necessary to estimate the engine displacement excitation which is the input to the model. Holt and Rao[14] assumed an excitation of amplitude 0.3 mm over the range 0 to 100 Hz and 0.01 mm over the range 100 to 200 Hz. Ohadi and Maghsoodi[15] assumed an excitation of amplitude 1.0 mm in the frequency range 0 to 6 Hz and 0.05 mm at higher frequencies. Lee et al.[3] measured the engine vibration amplitude at idling to be 0.22 mm. Kyprianou et. al.[16] assumed excitations with r.m.s amplitudes ranging from 0.005 mm at higher frequencies to 0.33 mm at lower frequencies. In this paper the engine vibration amplitude is assumed to be 0.5 mm at the idling frequency (20 Hz), decaying linearly to 0.1 mm at 100 Hz and then decreasing linearly to 0.05 mm at 1000 Hz. From this, the displacement requirement of the actuator is calculated from the transfer function (1) to be 1.6 mm at 20 Hz, 0.35 mm at 100 Hz, and 0.175 mm at 1000 Hz.

The transfer function between the actuator force and engine displacement can be written as

$$\frac{F}{X}(s) = \left(\frac{A_d}{A_e}\right) K_r, \tag{2}$$

from where the force requirement can be estimated as 26 N at idling. It is emphasized that these requirements are for complete cancellation of the engine vibrations. Actuators with capabilities lower than these could also provide significant (although not complete) vibration reduction. The force generation capability of the proposed

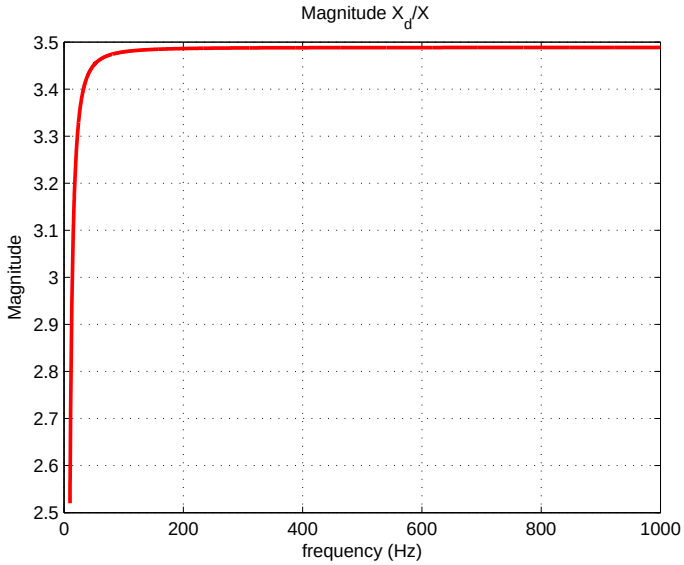

Figure 2. Frequency response (X_d/X) (magnitude only).

Table 1. Parameters of the active mount.

Parameter	Value
Main rubber stiffness (K_r)	127.4×10^3 N/m
Bulge stiffness of the rubber (K_b)	313.6×10^3 N/m
Compliance of the lower chamber (K_ϵ)	2.0 N/m
Equivalent cross-sectional area of the upper chamber (A_e)	4123 mm^2
Decoupler area	1662 mm^2
Cross-sectional area of the inertia track	50 mm^2
Fluid mass in the inertia track (m)	12.5 g
Damping coefficient in the inertia track	0.08 Ns/m

actuator will be decided by the dimensional constraints on the Terfenol-D rod. In this case a Terfenol-D rod with a diameter of 0.5 in and a length of 2 in has been chosen. This means that the expected blocked force generated by the rod is 4560 N (assuming E = 30 GPa) and its free stroke is 60 μm (assuming λ = 1200 ppm).

2.2 Actuator gain

One of the key factors in the performance of a displacement amplified actuator is the kinematic gain. The calculation of kinematic gain for an induced-strain actuator cannot be done simply by dividing the required displacement by the actuator free displacement. The maximum strain is obtained when the load is zero and the maximum load is supported when the displacement is zero. Thus, calculation of the kinematic gain must incorporate loading effects. Giurgiutiu et al.[17] established that to obtain maximum energy output from a displacement amplified induced-strain actuator, one must operate it at its optimal gain,

$$G_{opt} = 1/\sqrt{r}, \tag{3}$$

where r is the ratio of load stiffness to the smart material stiffness. The effective stiffness of the load and actuator is obtained by dividing (2) by (1). Figure 3 shows the load stiffness as a function of frequency. Since the actuator requirements are most stringent at the idling frequency, the stiffness match principle is enforced at that frequency and the value of the gain is found to be G_{opt} = 69. Thus the actuator is designed such that there is a fluid chamber with the large driving piston at one end and a small diameter load piston at the other. Figure 4 shows the physical actuator and a cutout showing the actuator components. The exact ratio of piston areas in this design is 69.6.

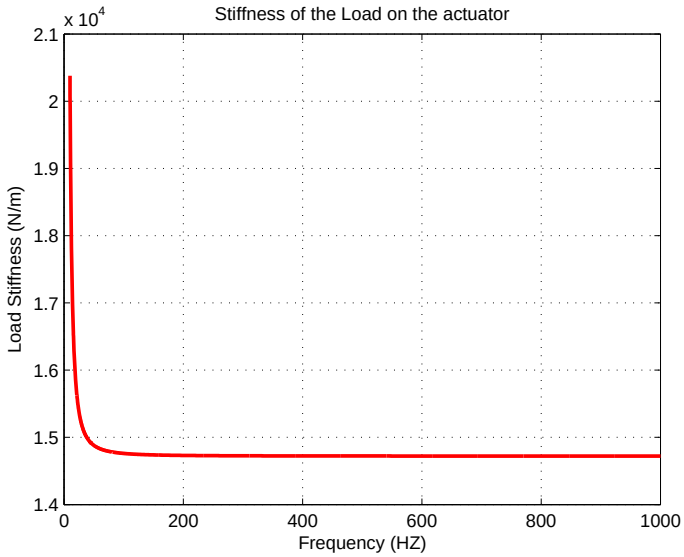

Figure 3. Load stiffness F/X_d (magnitude only).

2.3 Magnetic circuit and preload

The magnetic circuit consists of three cylindrical Alnico magnets with an ID of 1.125" and an OD of 1.5", a AWG 20 wire coil for generating the dynamic field, iron pieces for flux return and a Terfenol-D rod. The coil has an ID of 0.6" and an OD of 1". The permanent magnet provides the required magnetic bias to achieve bidirectional motion.

The mechanical preload on the Terfenol-D rod is obtained from two sources. First, through the wave spring on top whose force is then magnified by the fluid before being exerted on the Terfenol-D rod, and second through a disc spring located just above the magnetic circuit. The advantage of having a major part of the preload

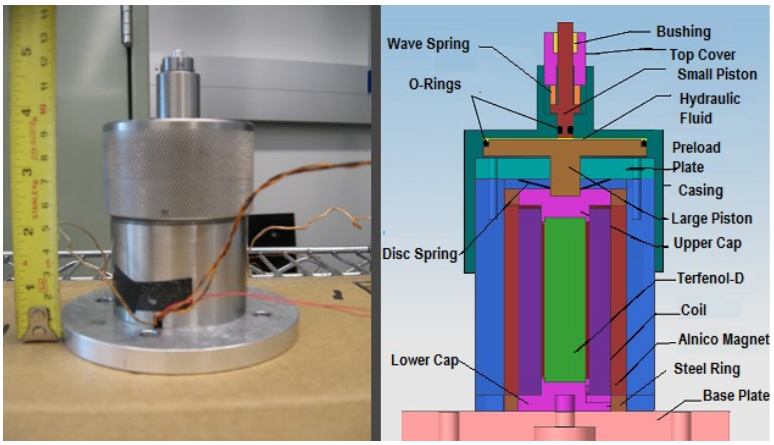

Figure 4. Physical actuator (left) and cutout (right).

Table 2. Different components used in the actuator.

Component	Specification
Length of Terfenol-D rod	2 in
Diameter of Terfenol-D rod	0.5 in
Alnico magnet (ID × OD × L)	(1.125 in × 1.5 in × 2.25 in)
Mass of larger Piston	74.67 g
Mass of smaller Piston	2.30 g
Volume of fluid(DTE 25)	1.30 c.c
Wave spring stiffness	2.27×10^3 N/m
Finger disc spring Stiffness	2.25×10^5 N/m

through the fluid is that the fluid remains in compression all the time thus reducing chances of cavitation. The fluid is sealed on both the ends by two dynamic o-rings (#6 for the smaller piston and #32 for the larger piston). Table 2 gives the specifications for the different components of the magneto-hydraulic actuator.

3. EXPERIMENTAL RESULTS

Both actuators are tested under mechanically-free (no external load) and mechanically-blocked conditions (no displacement of the output pushrod). The Magneto-Hydraulic Actuator (MHA) is driven by a current of 9 A pk-pk with no bias while the Commercial Mount Actuator (CMA) is driven at 6 A pk-pk with a 3 A dc bias. All tests in the frequency domain are obtained at constant current with the help of a controller and a feedback loop. Figure 5 shows a schematic of the experimental setup used to conduct the tests. The signal from the signal generator is amplified and fed to the MHA. The controller uses the amplifier's current monitor and a feedback loop to adjust the output of the signal generator in order to drive the MHA with a specified constant current.

3.1 Mechanically-free (unloaded) displacement

The free displacement was measured with a laser displacement sensor. Figure 6 shows the free displacement obtained from both of the actuators. It is emphasized that Figure 6 is obtained by running histogram tests at discrete frequencies from 10 to 500 Hz. This is so because the CMA hits a resonance around 100 HZ and the pushrod starts hitting the base of the mount creating a loud noise and erratic motion which makes it difficult to use the controller and carry out a stepped sine test. Driving the CMA at a lower drive level addresses this problem as shown in Figure 7.

The MHA generates a free displacement level of ±1 mm up to 200 Hz, and the phase decreases linearly up to 350 Hz. The CMA response shows a resonance at 100 Hz after which it rolls off quickly. An important aspect of

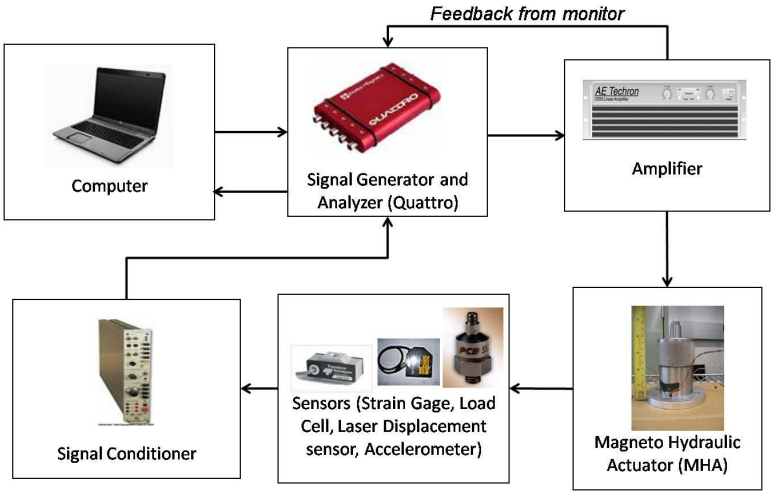

Figure 5. Schematic of the experimental setup.

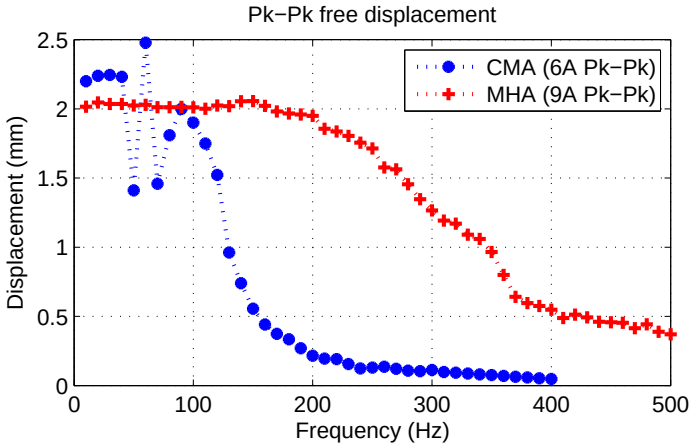

Figure 6. Displacement in mechanically-free (unloaded) conditions.

the performance of a mount actuator is that it should produce minimum higher-order harmonics. An actuator which has significant harmonic content can worsen the vibration isolation at higher frequencies when driven to suppress the fundamental mode of engine vibrations. Thus, for ease of control, the fundamental mode of the response must be as high as possible and the harmonics must be as low as possible. Figure 8 compares the free displacement orders of both of the actuators. The CMA exhibits a large resonance around 50 Hz. The MHA's higher-order displacements are significantly lower and flatter.

3.2 Mechanically-blocked (undeformed) force

The measurements under mechanically-blocked conditions were performed by blocking the output pushrod with a rigid fixture. These data provide a measure of the maximum force that can be obtained from the actuator. Figure 9 shows the response of both of the actuators. The MHA generates remarkably constant force over the frequency range considered. The CMA generates higher forces at the lower frequencies but the responses are nearly equal above 120 Hz. Similar to the free displacement, the blocked force order analysis was done to check for undesired higher harmonics in the generated force signals. Figure 10 shows that there is not much difference between the higher harmonic components of the two devices.

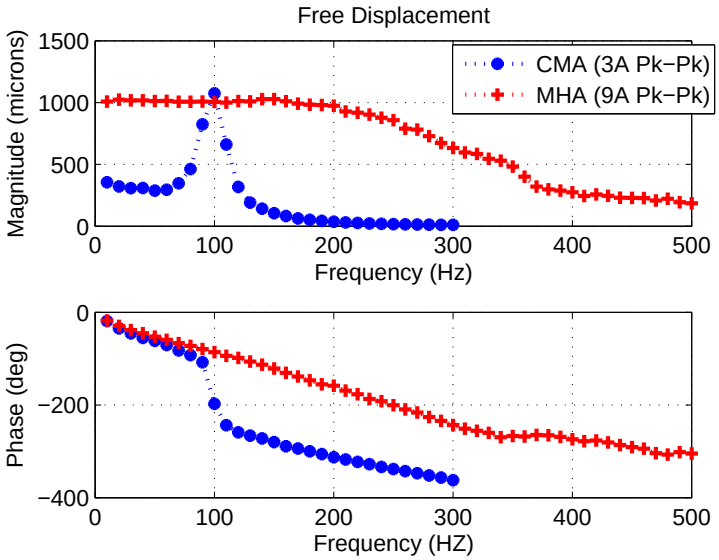

Figure 7. Displacement in mechanically-free (unloaded) conditions.

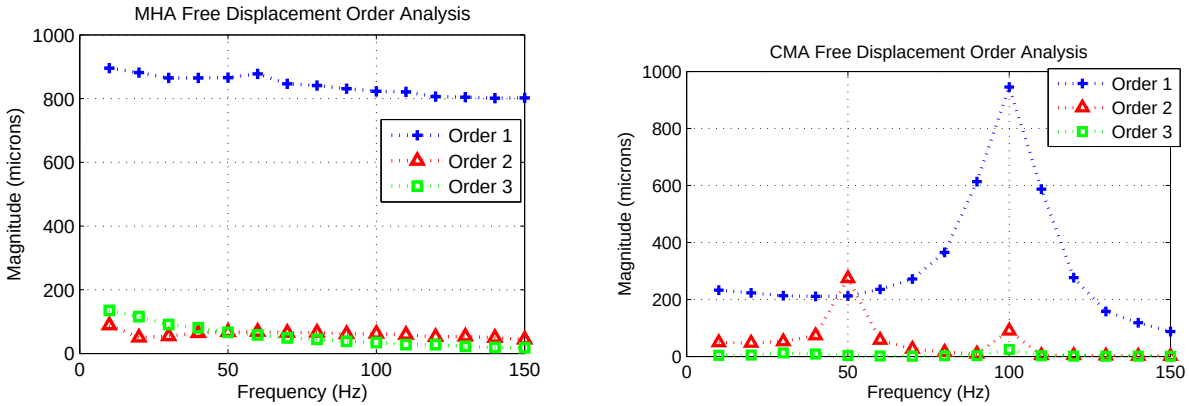

(a) (b)

Figure 8. Free displacement orders of (a) MHA and (b) CMA.

3.3 Power requirement

The MHA was driven with unbiased sinusoidal currents while the CMA was driven with sinusoidal currents and a bias magnetic field. However, in the power calculation the effect of bias was neglected since the bias in the CMA could also have been achieved by a permanent magnet as in the case of the MHA. The power is calculated with the help of current and voltage signals in the blocked condition. Figure 11 shows the power drawn by the two devices.

4. THEORY

A two-degree of freedom dynamic model was developed as shown in Figure 12. Assuming no compliance of the fluid chamber, at any given instant of time the volumetric displacement of the hydraulic fluid can be written as

$$\Delta V = A_p x_p - A_L x_L. \tag{4}$$

However, it is expected that the volumetric stiffness of the different elements in the fluid chamber would play a critical role in the performance of the actuator. Hence a volumetric stiffness coefficient (C_o) is introduced, to be

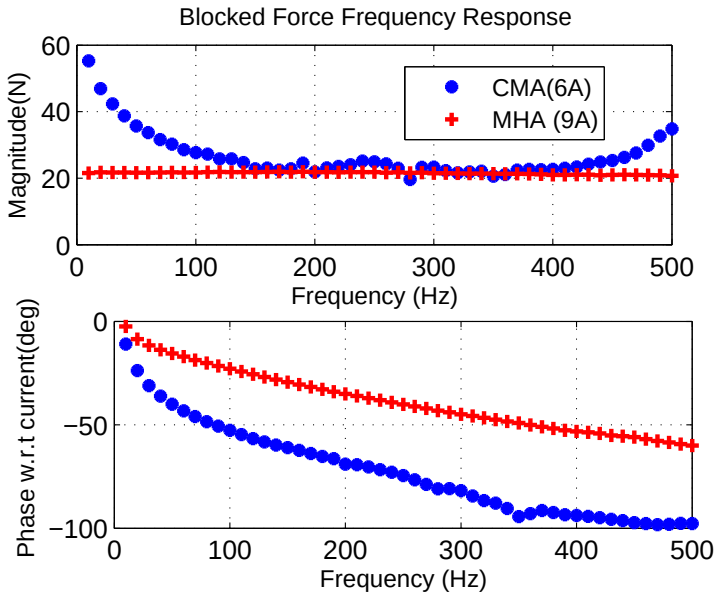

Figure 9. Measured force response in mechanically-blocked conditions.

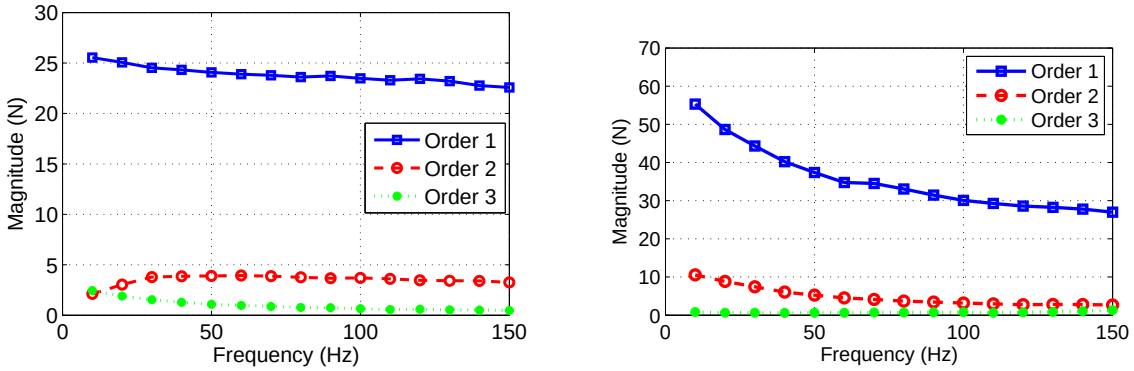

(a) (b)

Figure 10. Blocked force orders of (a) MHA and (b) CMA.

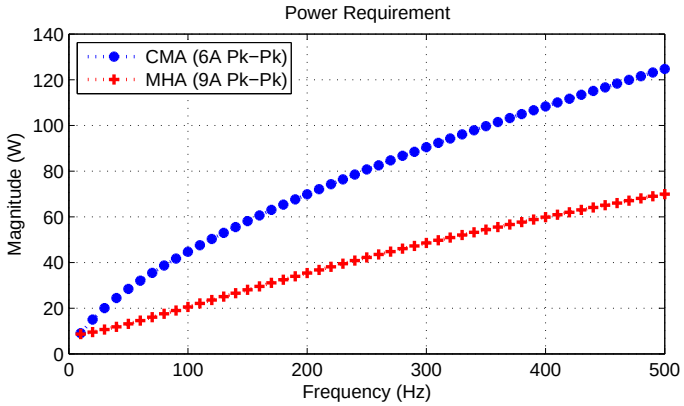

Figure 11. Comparison of power consumption of the MHA and CMA.

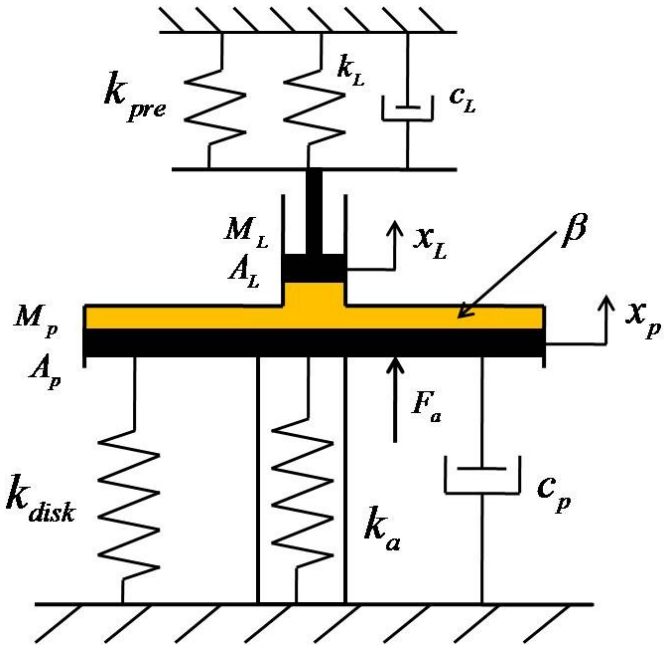

Figure 12. Schematic of the actuator model.

estimated experimentally. Now the volumetric change can be written as

$$\Delta V = A_p x_p - A_L x_L - \frac{\Delta p}{C_o}. \tag{5}$$

The pressure in the fluid can be linearized for small volumetric changes and can be written as

$$\Delta p = \beta \frac{\Delta V}{V_{ref}}. \tag{6}$$

Substitution of ΔV from (5) into (6) and solution for Δp gives

$$\Delta p = \underbrace{\left(\frac{C_o \beta}{C_o V_{ref} + \beta}\right)}_{\beta_{eff}} \left(A_p x_p - A_L x_L\right). \tag{7}$$

If the stiffness of the chamber is very large then the coefficient β_{eff} is approximately equal to β/V_{ref}. It is noted that β_{eff} is the effective volumetric modulus of the fluid and fluid chamber assembly and does not have the same units as β. A further reduction in the performance of the actuator is expected due to friction at the o-ring seals. Hence two friction forces fr_L and fr_p are assumed at the smaller and larger pistons respectively. The equations of motion can then be written as

$$M_p \ddot{x_p} + c_p \dot{x_p} + k_{p_{eff}} x_p + fr_p(sgn(\dot{x_p})) = \beta_{eff} \left(A_L x_L - A_p x_p\right) A_p + F_a, \tag{8}$$

$$M_L \ddot{x_L} + c_L \dot{x_L} + k_{L_{eff}} x_L + fr_L(sgn(\dot{x_L})) = \beta_{eff} \left(A_p x_p - A_L x_L\right) A_L. \tag{9}$$

The force generated by the Terfenol-D rod can be expressed in terms of the drive current as

$$F_a = \underbrace{(qK_a N)}_{\theta} I. \tag{10}$$

where q is the piezomagnetic coefficient and N is the number of turns in the driving coil. The electrical impedance of the device can be expressed as

$$U = RI + L_s \frac{dI}{dt} + \theta \frac{dx_p}{dt}, \tag{11}$$

in which the last term in the equation quantifies the effect of mechanical motion of the Terfenol-D rod on the electrical properties of the system. The inclusion of the signum functions in (8) and (9) makes the system nonlinear and hence the equations need to be solved numerically. The results for X_L, X_p and U/I obtained by solving the system of equations (8) - (11) are shown in Figures 13-15. The nonlinear model considering frictional forces provides a reasonably good description of the measurements. There are discrepancies in the phase which could be due to the assumed linear force-current relationship for the Terfenol-D rod.

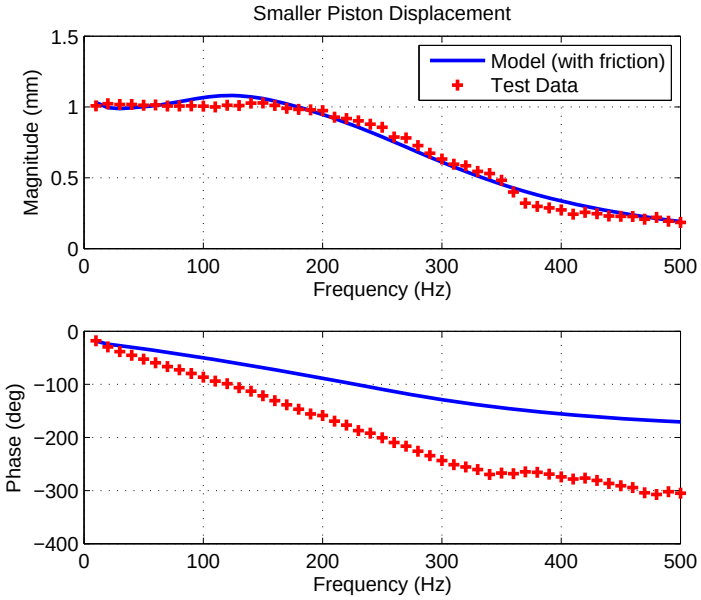

Figure 13. Bode plot of small piston displacement with respect to current.

5. CONCLUDING REMARKS

This paper presents the design and modeling of a hydraulically amplified magnetostrictive actuator, or Magneto-Hydraulic Actuator (MHA), developed for use in an active engine mount. The paper discusses the techniques used for estimating the actuator force and displacement requirement. The performance of the MHA is compared to that of a commercial mount actuator (CMA) currently in use. The actuators are tested at constant current in the free and blocked condition. The results show that the MHA is capable of providing a higher bandwidth of operation with a lower power consumption than the CMA. However, the MHA needs to be optimized to reduce the compliances in the load transmission path to increase its generated force levels. A nonlinear system model considering frictional forces is developed. The model calculations for the two piston displacements and electrical impedance provide a good match to the experimental results.

ACKNOWLEDGMENTS

We are grateful to the member organizations of the Smart Vehicle Concepts Center (www.SmartVehicleCenter.org) and the National Science Foundation Industry/University Cooperative Research Centers program for supporting this work.

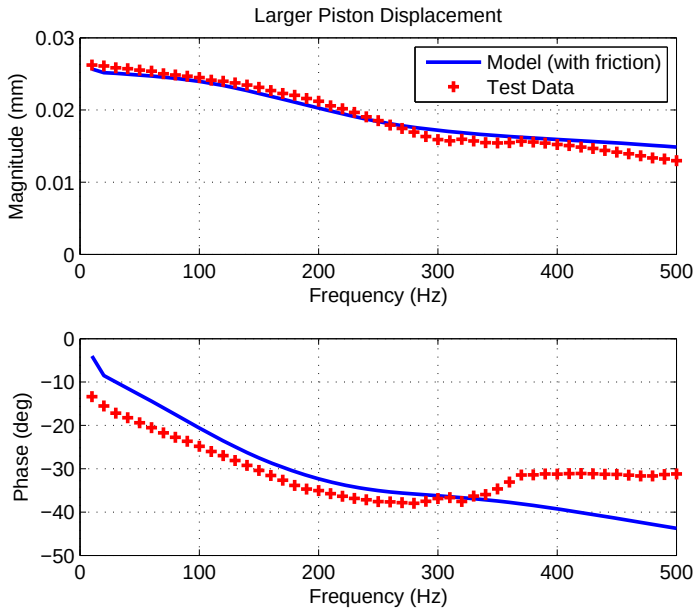

Figure 14. Bode plot of large piston displacement with respect to current.

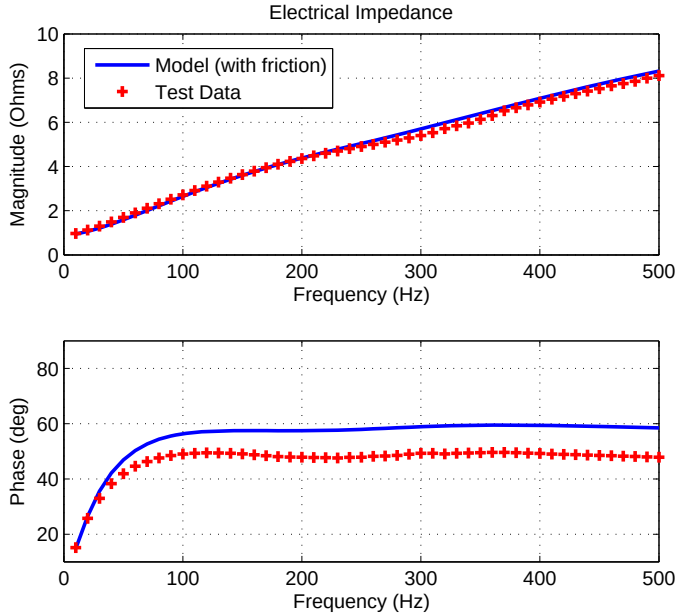

Figure 15. Bode plot of experimental and calculated electrical impedance.

REFERENCES

[1] Y. Yu, N. Naganathan, and R. Dukkipati, "A literature review of automobile engine mounting systems," in *Mechanisms and Machines Theory*, **36**, pp. 123–142, May 1999. PDF file.

[2] G. N. Jazar and F. Golnaraghi, "Engine mounts for automobile applications - a survey," *Shock and Vibration Digest* **34**, pp. 363–379, September 2002.

[3] Y. Lee and C. Lee, "Dynamic analysis and control of an active engine mount system," in *Proc Instn Mech Engrs Part D: J Automobile Engineering*, **216**, pp. 921–931, 2002.
[4] A. Gennesseaux, "A new generation of engine mounts," *SAE* (951296), 1995.
[5] C. Niezrecki, D. Brei, S. Balakrishnan, and A. Moskalik, "Piezoelectric actuation: State of the art," *Shock and Vibration Digest* **33**, pp. 269–280, July 2001.
[6] H.-S. Yoon, G. Washington, P. Eyabi, M. Radhamohan, S. W. Woodard, and R. Dayton, "Piezoelectric hydraulic pump development," *IEEE International Symposium on Industrial Electronics* **4**, pp. 2809–2813, July 2006.
[7] J. Ellison, J. Sirohi, and I. Chopra, "Design and testing of a bidirectional magnetostrictive-hydraulic hybrid actuator," in *Proc. SPIE, Smart Structures and Materials* **5390**, pp. 483–494, 2004.
[8] K. Bridger, J. M. Sewell, A. V. Cooke, J. L. Lutian, D. Kohlhafer, G. E. Small, and P. M. Kuhn, "High-pressure magnetostrictive pump development: a comparison of prototype and modeled performance," in *Proc. SPIE, Smart Structures and Materials* **5388**, pp. 246–257, 2004.
[9] L. D. Mauck and C. S. Lynch, "Piezoelectric hydraulic pump development," *Journal of Intelligent Material Systems and Structures* **11**, pp. 758–764, October 2000.
[10] J. Sirohi and I. Chopra, "Design and development of a high pumping frequency piezoelectric-hydraulic hybrid actuator," *Journal of Intelligent Material Systems and Structures* **14**, pp. 135–147, March 2003.
[11] M. J. Rupinsky and M. J. Dapino, "Smart material electrohydrostatic actuator for intelligent transportation systems," *Proc. ASME IMECE* (14542), 2006.
[12] T. Ushijima and S. Kumakawa, "Active engine mount with piezo-actuator for vibration control," *SAE* (930201), 1993.
[13] T. Shibayama, K. Ito, T. Gami, T. Oku, Z. Nakajima, and A. Ichikawa, "Active engine mount for a large amplitude of engine vibration," *SAE* (951298), 1995.
[14] J. Holt, M. Rao, J. Blough, and S. Gruenberg, "Time history-based excitation in the dynamic characterization of automotive elastomers," in *Proc. IMechE Part D: J. Automobile Engineering*, **221**, pp. 271–284, 2007.
[15] A. Ohadi and G. Maghsoodi, "Simulation of engine vibration on nonlinear hydraulic engine mounts," *Journal of Vibration and Accoustics* **129**, pp. 417–424, August 2007.
[16] A. Kyprianou, J. Giacomin, K. Worden, M. Heidrich, and J. Bocking, "Differential evolution based identification of automotive hydraulic engine mount model parameters," in *Proc. Instn. Mech. Engrs.*, **214**, 2000.
[17] V. Giurgiutiu, Z. Chaudhry, and C. Rogers, "Stiffness issues in the design of isa displacement amplification devices," in *Proc. SPIE*, **2443**, pp. 105–119, 1995.